9-11-2016

Atomistic-scale investigation of effective stress principle of saturated porous materials by molecular dynamics

Chao Zhang
Michigan Technological University

Zhen Liu
Michigan Technological University

Peng Deng
Colorado School of Mines

Recommended Citation

Zhang, C., Liu, Z., & Deng, P. (2016). Atomistic-scale investigation of effective stress principle of saturated porous materials by molecular dynamics. *Geophysical Research Letters, 43*(19), 10257-10265. http://doi.org/10.1002/2016GL070101
Retrieved from: https://digitalcommons.mtu.edu/cee-fp/47

Follow this and additional works at: https://digitalcommons.mtu.edu/cee-fp

 Part of the Civil and Environmental Engineering Commons

AGU PUBLICATIONS

Geophysical Research Letters

RESEARCH LETTER
10.1002/2016GL070101

Key Points:
- Molecular dynamics was explored as a tool to investigate the stress formulation in saturated porous materials
- The presence of pore water significantly alters the stress status of solids
- The intergranular stress is different from the effective stress

Correspondence to:
Z. Liu,
zhenl@mtu.edu

Citation:
Zhang, C., Z. Liu, and P. Deng (2016), Atomistic-scale investigation of effective stress principle of saturated porous materials by molecular dynamics, *Geophys. Res. Lett.*, *43*, 10,257–10,265, doi:10.1002/2016GL070101.

Received 19 JUN 2016
Accepted 8 SEP 2016
Accepted article online 11 SEP 2016
Published online 11 OCT 2016
Corrected 19 JAN 2017

This article was corrected on 19 JAN 2017. See the end of the full text for details.

Atomistic-scale investigation of effective stress principle of saturated porous materials by molecular dynamics

Chao Zhang[1], Zhen Liu[1], and Peng Deng[2]

[1]Department of Civil and Environmental Engineering, Michigan Technological University, Houghton, Michigan, USA, [2]Department of Civil and Environmental Engineering, Colorado School of Mines, Golden, Colorado, USA

Abstract The effective stress principle is one of the most fundamental concepts in the mechanics of porous materials. Several mathematical expressions have been proposed for this fundamental principle, leading to unsettled debates on the validity and applicability of the principle and its mathematical descriptions. Recent developments in atomistic modeling techniques make it possible to understand multiphase systems at the atomistic scale. In this paper, molecular dynamics simulation is explored as a tool to investigate the stress formulation in porous materials. A molecular dynamics framework, including molecular models of phases, interatomic potentials, initial configuration, and simulation procedure, is presented. Numerical simulations based on the framework preliminarily show the validity of the effective stress principle at the atomistic scale. Furthermore, the effectiveness of typical expressions for the principle is investigated.

1. Introduction

The effective stress principle, proposed by Karl von Terzaghi in the first half of the twentieth century, is the basis for understanding the mechanical behavior of saturated porous materials [*de Boer*, 1992]. The concept of the effective stress converts a multiphase, multistress porous medium to an equivalent single-phase medium, enabling the application of classical continuum mechanics to formulate the mechanical behavior of porous materials [*Khalili et al*., 2004, 2005]. According to *Lade and de Boer* [1997], the effective stress was defined as "the stress that controls the stress-strain, volume change and strength behavior of a given porous medium, independent of the magnitude of the pore pressure." The effective stress can be estimated by eliminating the pore fluid pressure component from the externally applied stress. A general formulation for the effective stress principle is expressed as [*Nuth and Laloui*, 2008; *Vlahinić et al*., 2011]:

$$\boldsymbol{\sigma}' = \boldsymbol{\sigma} - \eta u \boldsymbol{\delta}, \tag{1}$$

where $\boldsymbol{\sigma}'$ is the effective stress; $\boldsymbol{\sigma}$ is the externally applied stress; u is the pore fluid pressure; η is the coefficient; and $\boldsymbol{\delta}$ is the Kronecker delta.

The coefficient η was suggested to be 1.0 by *Terzaghi* [1923] with the assumptions of incompressible solid grains and incompressible fluids. The validity of $\eta = 1.0$ and the assumptions of incompressibility of the phases work well in most geotechnical applications. For example, the compressibilities of solid grains of most soils and water are negligible compared with those of their solid skeletons. Thus, the assumptions of incompressible solid grains and incompressible fluids hold for most soils, and $\eta = 1.0$ is valid. However, it has been recognized that these assumptions may not be applicable in a full range of porous materials or stress conditions [*Lade and De Boer*, 1997; *Nuth and Laloui*, 2008]. Various attempts have been made to extend the effective stress principle considering the compressibility of solid grains [*Biot and Willis*, 1957; *Skempton*, 1984; *Šuklje*, 1969]. Most of these studies confirmed equation (1) as a general formulation for the effective stress principle and recognized η as a function of parameters such as the porosity and the bulk modulus of solid grains rather than a constant [*Tuncay and Corapcioglu*, 1995]. A widely cited formulation of η was proposed by *Biot and Willis* [1957] as

$$\eta = 1 - \frac{K_b}{K_s}, \tag{2}$$

where K_b is the (drained) bulk modulus of the solid skeleton; and K_s is the bulk modulus of the solid grains. This formulation is widely accepted and frequently applied to rocks for which the values of K_b and K_s are

closer [*Geertsma*, 1956; *Nur and Byerlee*, 1971; *Skempton*, 1984; *Tuncay and Corapcioglu*, 1995]. Another widely-cited expression of η was proposed by *Šuklje* [1969], which explicitly accounts for the effect of the porosity as:

$$\eta = 1 - (1 - n)\frac{K_b}{K_s}, \tag{3}$$

where n is the porosity. Despite the acceptance, both formulations have been criticized [*Jaeger and Cook*, 1969; *Nur and Byerlee*, 1971; *Lade and De Boer*, 1997]. To date, the controversial issue in the exact expression of the coefficient η still remains unresolved. A comprehensive review for the expressions of η can be found in *Lade and de Boer* [1997].

In companion with the effective stress, the concept of the intergranular stress, the stress acting between neighboring particles, was introduced to understand the stress states of porous materials. But different statements of the intergranular stress were made by different researchers. For example, *Skempton* [1984] postulated that estimating the effective stress with the intergranular stress would cause unacceptable errors. Notwithstanding, *Mitchell and Soga* [2005] deduced that the intergranular stress was equal to the effective stress excluding physicochemical contributions. The intergranular stress concept is still widely used to deduce the effective stress for unsaturated porous materials [*Vlahinić et al*., 2011]. To date, the exact relationship between the intergranular stress and the effective stress has not been identified yet.

The aforementioned two issues, i.e., the exact formulation of the effective stress principle and the exact relationship between the intergranular stress and the effective stress, prevent the further understanding of porous materials and may hinder the application of the effective stress principle to advanced porous materials, especially those with more phases and components. Experimental techniques still show difficulties in helping resolve the issues because the available experimental apparatuses and materials are not sensitive enough to calibrate the formulations of η. Also, it is extremely difficult to remove geometric and material nonlinearities when conducting quantitative experimental studies. Therefore, clarification of the controversies possibly needs to rely on the innovations in other aspects, such as computer simulation techniques. Recent developments in molecular dynamics (MD) enable us to investigate complex physical phenomena in multiphase systems, such as stress states, phase equilibrium, and transition [*Liu et al*., 2004; *Luan and Robbins*, 2005; *Tadmor and Miller*, 2011; *Cheng and Robbins*, 2014; *Zhang et al*., 2016]. It is very likely that MD can serve as a strong candidate technique for seeking new insights into the effective stress principle and thus probably helps resolve the historical issues. This study is a preliminary investigation intended for exploring this possibility. For this purpose, an MD framework is proposed to evaluate the validity of the effective stress principle and to help clarify unresolved controversial issues.

2. Theoretical Basis

Since the effective stress cannot be directly measured [*Toker et al*., 2014], it is crucial to select a measurable variable to reflect its magnitude. As an extreme case of the effective stress principle, the effective stress in the dry porous medium is equal to the externally applied stress [*Nuth and Laloui*, 2008]:

$$\boldsymbol{\sigma}' = \boldsymbol{\sigma}. \tag{4}$$

The externally applied stress in the dry porous medium can be related to the pore water pressure and externally applied stress in the same porous medium saturated with water via a "superposition" as shown in Figure 1. Accordingly, the effective stress of the saturated porous medium is equal to the externally applied stress of the dry porous medium under the same volumetric strain. Therefore, the externally applied stress of the saturated porous medium ($\boldsymbol{\sigma}$) can be decomposed into an effective stress component ($\boldsymbol{\sigma}'$, equivalent to the externally applied stress of the dry porous medium) and a pore water pressure component (ηu). All of the above stresses are measurable. Thus, the coefficient η can be directly determined as

$$\eta = \frac{\boldsymbol{\sigma} - \boldsymbol{\sigma}'}{u\boldsymbol{\delta}}, \tag{5}$$

and in a plain strain case (Figure 1),

$$\eta = \frac{\sigma_m - \sigma_m'}{u}, \tag{6}$$

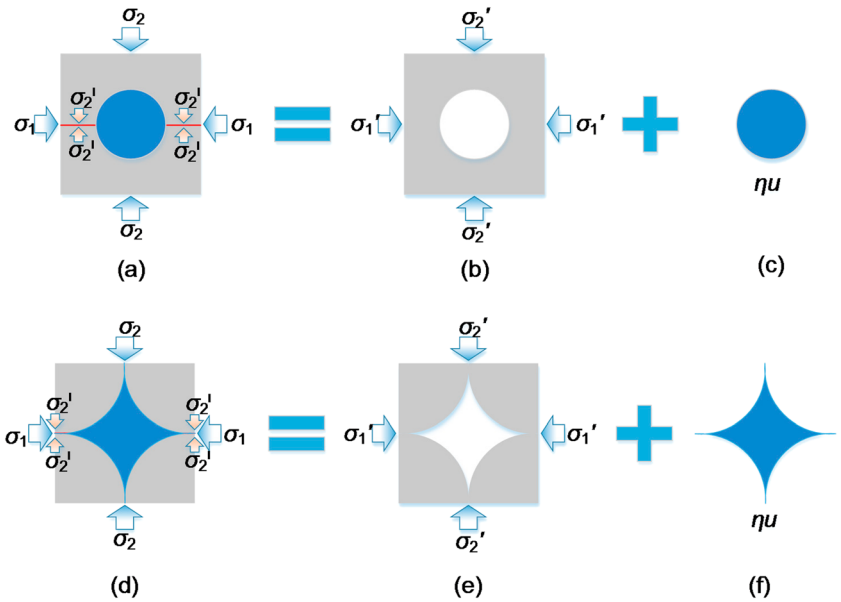

Figure 1. Illustration of the effective stress principle with two typical conceptual models for porous materials for (a–c) the solid with circular pores and (d–f) the cubic packing granular medium. The grey and blue regions represent solid and pore water, respectively. The lines in the red color denote the cross section of contact area. The arrows in the amber color represent the intergranular stress.

where $\sigma_m = (\sigma_1 + \sigma_2)/2$ is the mean externally applied stress and $\sigma_m' = (\sigma_1' + \sigma_2')/2$ is the mean effective stress. Based on the ergodicity hypothesis, these macroscopic stresses were derived from time-average atomistic stresses. Detailed formulations of atomistic stresses can be found in *Thompson et al.* [2009]. MD simulation is a modeling technique primarily applying to the nanoscale. As a result, the modeling capacity is limited to several representative volume elements (RVEs) considering the computational cost. Nevertheless, with the aid of periodic boundary conditions, MD can model material behavior by investigating only one RVE. Two typical RVEs were considered as two common cases of porous materials in MD simulations. One is a solid with circular pores (Figures 1a–1c) which is widely adopted to represent porous materials like rocks and concrete. The other is a cubic packing granular medium (Figures 1d–1f) which is predominantly used to derive or interpret general physical models for granular materials. As illustrated in Figures 1a and 1d, the intergranular stress (σ_2^I) can be directly measured as the normal stress over the contact area.

3. Interatomic Potentials

Interatomic potentials are constitutive relations for molecular systems and thus should be well defined. Three types of interatomic potentials need to be considered for the molecular system simulating the solid with circular pores: water-water interaction, solid-solid interaction, and solid-water interaction. As for the molecular system simulating the cubic packing granular medium, an extra contact model is required to depict the contact force between solid particles.

3.1. Water-Water Interaction

A relatively large MD model was used to evaluate the effective stress principle, requiring tens of thousands of atoms. The major concern for this kind of molecular system is the computational cost. To facilitate parametric studies, it is necessary to limit the computational time of one case study to a couple of weeks. Various conventional atomistic models have been proposed for the water-water interaction [*Berendsen et al.*, 1981, 1987; *Jorgensen et al.*, 1983]. However, these conventional models usually employ the particle-particle, particle-mesh method [*Hockney and Eastwood*, 1988] to tackle with long-range Coulombic forces, which is computationally expensive. To speed up simulations, a monoatomic water (mW) model developed by *Molinero and Moore* [2008] was selected to model the water-water interaction by taking advantage of its low computational costs. The mW model has been successfully implemented to investigate the freezing and melting of nanoconfined water [*Moore et al.*, 2012], sorption isotherms of water in nanopores

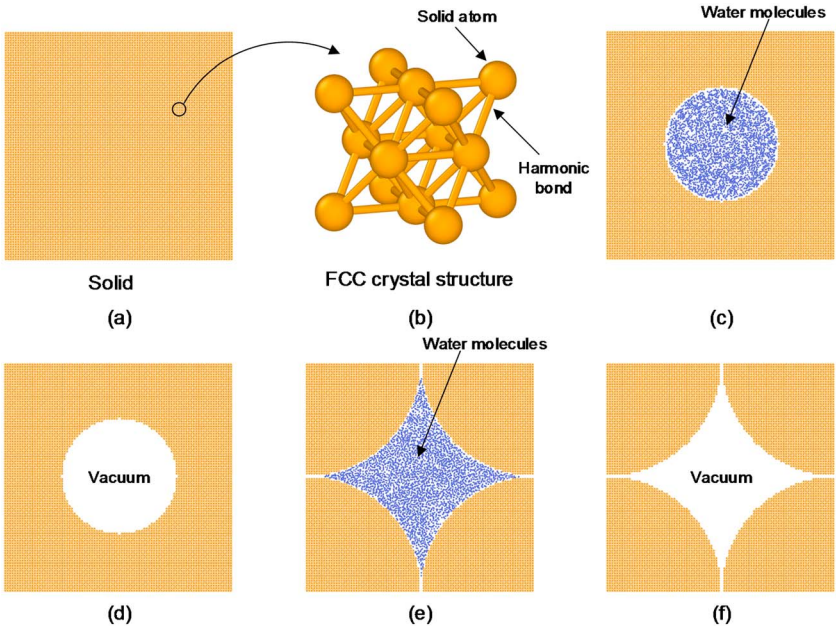

Figure 2. Initial configurations for MD simulations: (a) the pure solid to calculate the bulk modulus of solid grains, (b) MD representation of the solid with the FCC crystal structure, (c) the saturated solid with circular pores, (d) the dry solid with circular pores, (e) the saturated cubic packing granular medium, and (f) the dry cubic packing granular medium. The amber and blue points represent solid atoms and water molecules, respectively.

[*de la Llave et al.*, 2012], and vapor pressure of nanodroplets [*Factorovich et al.*, 2014]. In the mW model, the water-water interaction is modeled by only short-range interactions based on similarities between water and silicon and is formulated using the Stillinger-Weber potential [*Stillinger and Weber*, 1985] as

$$E = \sum_i \sum_{j>i} \phi_2(r_{ij}) + \sum_i \sum_{j\neq i} \sum_{k>j} \phi_3(r_{ij}, r_{ik}, \theta_{ijk}), \tag{7}$$

$$\phi_2(r_{ij}) = A\epsilon_1 \left[B\left(\frac{r_{\min}}{r_{ij}}\right)^{p_{ij}} - \left(\frac{r_{\min}}{r_{ij}}\right)^{q_{ij}} \right] \exp\left(\frac{r_{\min}}{r_{ij} - a r_{\min}}\right), \tag{8}$$

$$\phi_3(r_{ij}, r_{ik}, \theta_{ijk}) = \lambda\epsilon_1 (\cos\theta_{ijk} - \cos\theta_0)^2 \exp\left(\frac{\gamma r_{\min}}{r_{ij} - a r_{\min}} + \frac{\gamma r_{\min}}{r_{ik} - a r_{\min}}\right), \tag{9}$$

where r_{ij} is the distance between atom i and atom j; θ_{ijk} is the angle between the vector r_{ij} and vector r_{ik}; and the other parameters are constants: $A = 7.049556277$, $B = 0.6022245584$, $p_{ij} = 4$, $q_{ij} = 0$, $\gamma = 1.2$, $a = 1.8$, $\theta_0 = 109.47°$, $\lambda = 23.15$, $r_{\min} = 2.3925$ Å, and $\epsilon_1 = 6.189$ kcal/mol.

3.2. Solid-Solid Interaction

In Figure 2b, a face-centered-cubic (FCC) crystal structure is chosen to model the solid as suggested by *Luan and Robbins* [2005]. In order to create a perfectly elastic solid, harmonic bonds were added between solid atoms. The interaction potential between solid atoms is expressed as

$$E = K(r_{ij} - r_0)^2, \tag{10}$$

where K is the spring constant and selected as 6.0 kcal/mol to create a relatively compressible solid and $r_0 = 3.1$ Å is the equilibrium interaction distance.

3.3. Solid-Water Interaction

The solid-water interaction was also modeled by the Stillinger-Weber potential. All the parameters except λ, $r_{\min}$, and ϵ_1 were identical to those in the mW model. To create a relatively hydrophilic solid and prevent the diffusion of water molecules into the solid, the values of λ, $r_{\min}$, and ϵ_1 were determined as 0.0, 32 Å, and 0.6 kcal/mol, respectively [*Moore et al.*, 2012].

3.4. Contact Model

The contact between solid particles needs to be considered for the cubic packing granular medium. A truncated and shifted 12-6 Lennard-Jones potential was selected for this purpose as suggested by *Luan and Robbins* [2005]. This potential is mathematically formulated as

$$E = 4\epsilon_2\left[\left(\frac{r_{\min}'}{r_{ij}}\right)^{12} - \left(\frac{r_{\min}'}{r_{ij}}\right)^{6} - \left(\frac{r_{\min}'}{r_c}\right)^{12} + \left(\frac{r_{\min}'}{r_c}\right)^{6}\right] \tag{11}$$

where $\epsilon_2 = 2.02$ kcal/mol is the characteristic interaction energy, $r_{\min}' = 3.1$ Å is the distance corresponding to the minimal interaction energy, and $r_c = 2^{1/6} r_{\min}'$ is the cutoff distance.

4. Simulation Details

4.1. Initial Configuration

Figures 2c and 2d illustrate the initial configurations of the saturated and dry solids with circular pores, respectively. The width and height of the system are 20.17 nm. The circular pore with a diameter of 10.0 nm is located at the center of the system. The initial configurations of the saturated and dry cubic packing granular media are shown in Figures 2e and 2f. The dimensions of the system are also 20.17 nm, while the radius of solid particles is 10.0 nm. In Figures 2c and 2e, the pores are fully filled with water molecules. The initial configuration of water molecules should be carefully established because the excessively close distances between molecules would generate unacceptable large interatomic interactions and disrupt simulations. For this purpose, the packing of water molecules in initial configurations were optimized using PACKMOL [*Martínez et al*., 2009]. An iterative procedure was developed to determine the numbers of water molecules (n_w) for filling the pores. In this procedure, n_w is first estimated as the ratio of the pore volume to the volume occupied by one water molecule in bulk water (about 0.0299 nm^3). Then, the average density of water is calculated by equilibrating the molecular systems under an *NVT* ensemble at a constant temperature of 300 K over 5 ns. If this obtained average density is smaller than the density of bulk water (1000 kg/m^3), n_w increases; otherwise, n_w decreases. Repeat this process until an average density closest to 1000 kg/m^3 is achieved. In this study, n_w was determined as 3544 for the solid with circular pores and 4039 for the cubic packing granular medium. In addition, n_w was varied as 3543, 3544, and 3545 for the solid with circular pores and 4038, 4039, and 4040 for the cubic packing granular medium to check the stability of the proposed method.

The bulk modulus of the solid skeleton (K_b) can be conveniently obtained with the simulation cases in Figures 2d and 2f. The bulk modulus of the solid grains (K_s) is also required to evaluate the accuracy of existing expressions such as equations (2) and (3). This quantity was obtained with a pure solid simulation case shown in Figure 2a. The dimensions of the pure solid simulation case are also 20.17 nm.

4.2. Simulation Procedure

The simulations were performed under an *NVT* ensemble with a constant temperature of 300 K. The loading processes were achieved through increasing the normal strains of the systems, i.e., ε_1 and ε_2, step by step. Each step consisted of one loading stage and one subsequent equilibrium stage. During the loading stage, the normal strains were increased at a strain rate of -1.0×10^{-7} fs^{-1}. Newton's equations of motion were integrated with a time step of 0.1 fs. During the equilibrium stage, the loading was terminated, and the molecular systems were equilibrated for 5.0 ns with a time step of 5.0 fs. The molecular trajectories in the last 2.5 ns of the equilibrium stage were recorded to compute stress contours. Such a loading procedure was repeated 10 times for all the simulation cases. Therefore, the stress contours were obtained at the normal strain from -0.005 to -0.05 with an interval of -0.005. MD simulations were conducted using Large-scale Atomic/Molecular Massively Parallel Simulator (LAMMPS) [*Plimpton*, 1995; *Plimpton et al*., 2007] and visualized using Open Visualization Tool [*Stukowski*, 2010]. The boundary conditions were set as periodic. To avoid rigid movements, the solid atoms in the corners of the systems were fixed during the equilibrium stage.

5. Results

The contours of the mean stress and pore water pressure of the solid with circular pores are shown in Figure 3. Some water molecules diffused into the solids due to the instability of the MD simulations during the initial

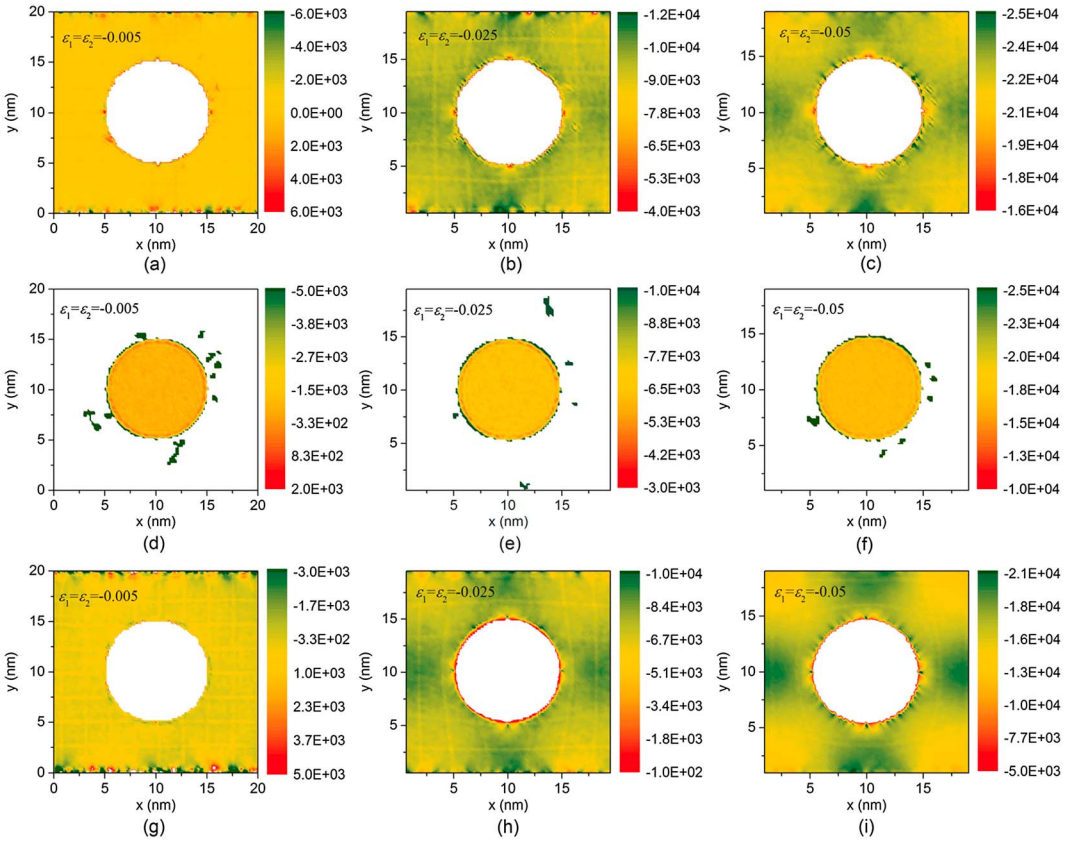

Figure 3. The mean stress and pore water pressure contours of the solid with circular pores for the following: mean stresses of the saturated solid with normal strains of (a) −0.005, (b) −0.025, and (c) −0.05; pore water pressures in the saturated cases with normal strains of (d) −0.005, (e) −0.025, and (f) −0.05; and mean stresses of the dry solid with normal strains of (g) −0.005, (h) −0.025, and (i) −0.05. The units of stress or pressure are atm.

equilibrium process. As a result, some pore water pressure values are observed in the solid region in Figures 3d–3f. However, only a minor of portion of water molecules (i.e., not more than five water molecules) diffused into the solid region. Thus, this diffusing phenomena has negligible effects on the stress states of the solid region, as shown in Figures 3g–3i. Evidently, the presence of the pore water alters the stress states in the RVE. The mean stress of the solid in the saturated case is more uniform than that in the dry case. In Figures 3d–3f, a noticeable sudden change in the pore water pressure is observed along the solid-water interface, resulting from the solid-water interaction, i.e., adsorption.

Figure 4 illustrates the stress and pressure contours of the saturated and dry cubic packing granular media. Some pore water pressure spots outside of the pore water region in Figures 4d–4e are caused by the water molecules diffusing into the solid. In Figures 4a–4c and 4g–4i, the contact area between the particles expands with increasing mean strains. Comparing Figures 4a–4c with Figures 4g–4i, the mean stresses within the solid region in the saturated case are much larger than those in the dry case, while the mean stresses within the contact region are close. The sudden change in the pore water pressure along the solid-water interface is greater than that in Figure 3, attributable to the fact that adsorption is more significant in angular pores than circular pores [*Tuller et al*., 1999].

The coefficient η calculated from the MD simulations was compared with those calculated with equations (2) and (3) in Figures 5a and 5b. The coefficient η calculated by taking the intergranular stress as the effective stress (referred to as "the calculation by intergranular stress") was also included in Figures 5a and 5b. K_b and K_s were calculated from the MD simulations as mentioned in section 4.1, while n was calibrated based on the initial configuration. Figures 5c and 5d show the comparisons of the intergranular stress and effective stress. As for the solid with circular pores, in Figure 5a, the predictions with the two equations are close to the

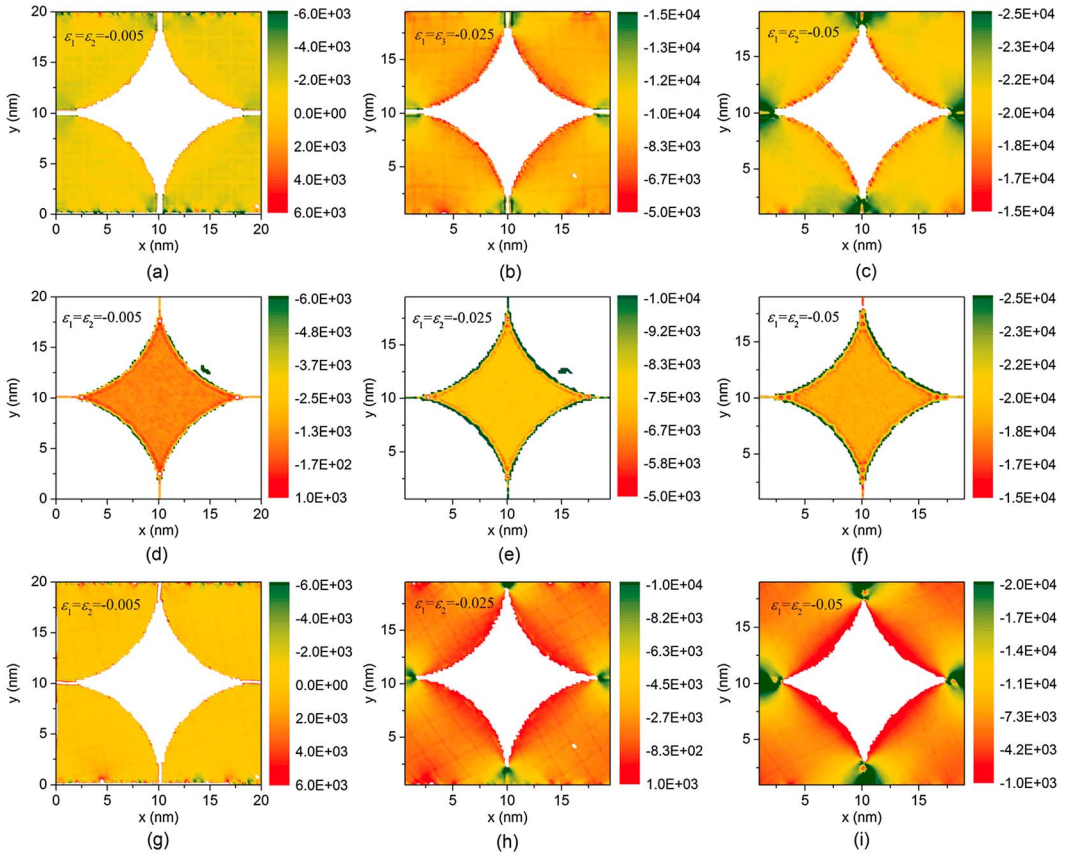

Figure 4. The mean stress or pore water pressure contours of the cubic packing granular medium for the following: mean stresses of the saturated solid with normal strains of (a) −0.005, (b) −0.025, and (c) −0.05; pore water pressures in the saturated cases with normal strains of (d) −0.005, (e) −0.025, and (f) −0.05; and mean stresses of the dry solid with normal strains of (g) −0.005, (h) −0.025, and (i) −0.05. The units of stress or pressure are atm.

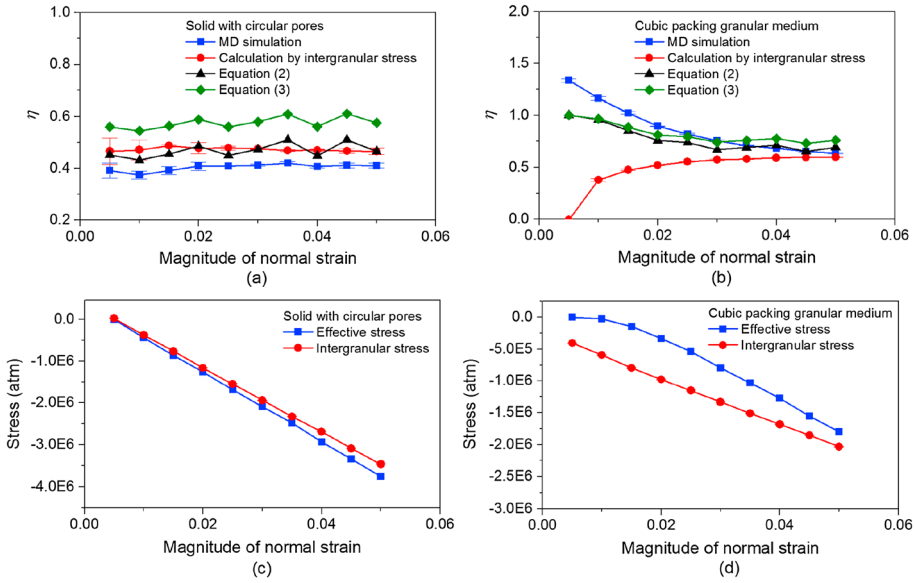

Figure 5. Comparisons of the coefficient η determined from MD simulations, calculation by intergranular stress, Equations (2) and (3) for (a) the solid with circular pores and (b) the cubic packing granular medium. The error bars are obtained by using three different initial water configurations. Comparisons of the intergranular stress and the effective stress for (c) the solid with circular pores and (d) the cubic packing granular medium.

MD simulation results albeit that the predictions are higher than the MD simulations. In addition, the predictions with equation (3) agree very well with the calculation by intergranular stress, suggesting that equations (3) can well predict the intergranular stress states in this kind of porous material. In Figure 5c, both the intergranular stress and effective stress are approximately proportional to the normal strain. Nevertheless, their stiffness values (stress over normal stain) are slightly different from each other, indicating their distinct physical mechanisms.

As for the cubic packing granular medium, in Figure 5b, the MD simulation results are higher than the predictions with the two equations at small strain magnitudes (i.e., 0.005–0.02) but close to the predictions at large strain magnitudes (i.e., 0.025–0.05). Also, the calculation by intergranular stress significantly differs from the predictions with the two equations, and the differences decrease with increasing strain magnitudes. In Figure 5d, a similar trend is observed. These differences at small strain magnitudes may be explained by the presence of adsorbed water in the contact region. Before the solid particles get into good contact with their neighboring particles, there are slits between them as shown in Figures 4a and 4g. As for the dry case, these slits make the contact region less stiff than the solid region, and as a result, the compressive strains concentrate in the contact region. With increasing strain magnitudes, these slits close; the solid particles get into good contact with each other; and consequently, the stiffness of the contact region is comparable to that of the solid region. As a result, the effective stress-normal strain curve exhibits nonlinearity: the corresponding stiffness increases with the strain magnitudes. As for the saturated case, these slits are filled with adsorbed water molecules as illustrated in Figure 4d. No strain concentrations would occur in the contact region. Hence, the intergranular stress-normal strain curve is almost linear. Therefore, it can be concluded that the intergranular stress and the effective stress are distinctively different. Also, it may be inferred that the formulations of the effective stress may depend on the wetting and loading histories in this kind of porous materials.

6. Conclusions

This study pioneers the application of molecular dynamics simulation as an innovative computational approach to investigate the stress distribution and formulation in porous materials. The study succeeded in obtaining measurable stresses and mechanical properties to evaluate the mathematical formulation of the effective stress principle based on the proposed framework. It is shown that the presence of pore water significantly alters the stress states of the solids in the two typical cases of porous materials. The coefficient η calculated from MD is different from but close to the predictions with the two widely cited expressions. The simulation results also indicate that the intergranular stress is different from the effective stress. The proposed framework has the potential to be extended as a major tool for investigating the stress states of more complex material systems, such as unsaturated soils or porous materials with even more phases.

Acknowledgments
The financial support from the National Science Foundation (NSF CMMI 1562522) is gratefully acknowledged. We also acknowledge Superior, a high-performance computing cluster at Michigan Technological University, for providing computational resources to fulfill this study. The insightful and constructive comments provided by the anonymous reviewers are very much appreciated by the authors. Data used in this study are available from the corresponding author.

References

Berendsen, H. J., J. P. Postma, W. F. van Gunsteren, and J. Hermans (1981), Interaction models for water in relation to protein hydration, in *Intermolecular Forces, Proceedings of the Fourteenth Jerusalem Symposium on Quantum Chemis try and Biochemistry*, pp. 331–342, Springer, Jerusalem, Israel.

Berendsen, H. J. C., J. R. Grigera, and T. P. Straatsma (1987), The missing term in effective pair potentials, *J. Phys. Chem.*, *91*(24), 6269–6271.

Biot, M. A., and D. G. Willis (1957), The elastic coefficients of the theory of consolidation, *J. Appl. Mech.*, *24*, 594–601.

Cheng, S., and M. O. Robbins (2014), Capillary adhesion at the nanometer scale, *Phys. Rev. E*, *89*(6), 062402.

De Boer, R. (1992), Development of porous media theories—A brief historical review, *Trans. Porous Media*, *9*(1–2), 155–164.

de la Llave, E., V. Molinero, and D. A. Scherlis (2012), Role of confinement and surface affinity on filling mechanisms and sorption hysteresis of water in nanopores, *J. Phys. Chem. C*, *116*(2), 1833–1840.

Factorovich, M. H., V. Molinero, and D. A. Scherlis (2014), Vapor pressure of water nanodroplets, *J. Am. Chem. Soc.*, *136*(12), 4508–4514.

Geertsma, J. (1956), The effect of fluid pressure decline on volumetric changes of porous rocks, Paper presented at Petroleum Branch Fall Meeting in Los Angeles.

Hockney, R. W., and J. W. Eastwood (1988), *Computer Simulation Using Particles*, CRC Press, U. K., and New York.

Jaeger, J. C., and N. G. W. Cook (1969), *Fundamentals of Rock Mechanics*, Methuen, London.

Jorgensen, W. L., J. Chandrasekhar, J. D. Madura, R. W. Impey, and M. L. Klein (1983), Comparison of simple potential functions for simulating liquid water, *J. Chem. Phys.*, *79*(2), 926–935.

Khalili, N., F. Geiser, and G. E. Blight (2004), Effective stress in unsaturated soils: Review with new evidence, *Int. J. Geomech.*, *4*(2), 115–126.

Khalili, N., R. Witt, L. Laloui, L. Vulliet, and A. Koliji (2005), Effective stress in double porous media with two immiscible fluids, *Geophys. Res. Lett.*, *32*, L15309, doi:10.1029/2005GL023766.

Lade, P. V., and R. De Boer (1997), The concept of effective stress for soil, concrete and rock, *Geotechnique*, *47*(1), 61–78.

Liu, W. K., E. G. Karpov, S. Zhang, and H. S. Park (2004), An introduction to computational nanomechanics and materials, *Comput. Methods Appl. Mech. Eng.*, *193*(17), 1529–1578.

Luan, B., and M. O. Robbins (2005), The breakdown of continuum models for mechanical contacts, *Nature*, *435*(7044), 929–932, doi:10.1038/nature03700.
Martínez, L., R. Andrade, E. G. Birgin, and J. M. Martnez (2009), PACKMOL: A package for building initial configurations for molecular dynamics simulations, *J. Comput. Chem.*, *30*(13), 2157–2164.
Mitchell, J. K., and K. Soga (2005), *Fundamentals of Soil Behavior*, John Wiley, Hoboken, N. J.
Molinero, V., and E. B. Moore (2008), Water modeled as an intermediate element between carbon and silicon, *J. Phys. Chem. B*, *113*(13), 4008–4016.
Moore, E. B., J. T. Allen, and V. Molinero (2012), Liquid-ice coexistence below the melting temperature for water confined in hydrophilic and hydrophobic nanopores, *J. Phys. Chem. C*, *116*(13), 7507–7514.
Nur, A., and J. Byerlee (1971), An exact effective stress law for elastic deformation of rock with fluids, *J. Geophys. Res.*, *76*, 6414–6419, doi:10.1029/JB076i026p06414.
Nuth, M., and L. Laloui (2008), Effective stress concept in unsaturated soils: Clarification and validation of a unified framework, *Int. J. Numer. Anal. Methods Geomech.*, *32*(7), 771–801.
Plimpton, S. (1995), Fast parallel algorithms for short-range molecular dynamics, *J. Comput. Phys.*, *117*(1), 1–19.
Plimpton, S., P. Crozier, and A. Thompson (2007), *LAMMPS-large-scale Atomic/molecular Massively Parallel Simulator*, 18 pp., Sandia National Laboratories, Albuquerque, N. M., and Livermore, Calif.
Skempton, A. (1984), Effective stress in soils, concrete and rocks, *Sel. Pap. Soil Mech.*, *1032*, 4–16.
Stillinger, F. H., and T. A. Weber (1985), Computer simulation of local order in condensed phases of silicon, *Phys. Rev. B*, *31*(8), 5262.
Stukowski, A. (2010), Visualization and analysis of atomistic simulation data with OVITO—The Open Visualization Tool, *Modell. Simulation Mater. Sci. Eng.*, *18*(1), 015012.
Šuklje, L. (1969), *Rheological Aspects of Soil Mechanics*, Wiley-Intersci.
Tadmor, E. B., and R. E. Miller (2011), *Modeling Materials: Continuum, Atomistic and Multiscale Techniques*, Cambridge Univ. Press.
Terzaghi, K. V. (1923), Die berechnung der durchlassigkeitsziffer des tones aus dem verlauf der hydrodynamischen spannungserscheinungen, in *Sitzungsberichte der Akademie der Wissenschaften in Wien, Mathematisch-Naturwissenschaftliche Klasse, Abteilung IIa*, vol. 132, pp. 125–138, Vienna.
Thompson, A. P., S. J. Plimpton, and W. Mattson (2009), General formulation of pressure and stress tensor for arbitrary many-body interaction potentials under periodic boundary conditions, *J. Chem. Phys.*, *131*(15), 154107.
Toker, N. K., J. T. Germaine, and P. J. Culligan (2014), Effective stress and shear strength of moist uniform spheres, *Vadose Zone J.*, *13*(5).
Tuller, M., D. Or, and L. M. Dudley (1999), Adsorption and capillary condensation in porous media: Liquid retention and interfacial configurations in angular pores, *Water Resour. Res.*, *35*, 1949–1964, doi:10.1029/1999WR900098.
Tuncay, K., and M. Y. Corapcioglu (1995), Effective stress principle for saturated fractured porous media, *Water Resour. Res.*, *31*, 3103–3106, doi:10.1029/95WR02764.
Vlahinić, I., H. M. Jennings, J. E. Andrade, and J. J. Thomas (2011), A novel and general form of effective stress in a partially saturated porous material: The influence of microstructure, *Mech. Mater.*, *43*(1), 25–35.
Zhang, C., Z. Liu, and P. Deng (2016), Contact angle of soil minerals: A molecular dynamics study, *Comp. Geotech.*, *75*, 48–56.

Erratum

In the originally published version of this paper, the epsilon symbols appearing in equations 8, 9, and 11 were not correctly typeset. These errors have since been corrected and this version may be considered the authoritative version of record.